Research Article | Vol. 29, No. 15 / 19 July 2021 / Optics Express 23500
Optics EXPRESS

Absolute calibration of a single-photon avalanche detector using a bright triggered single-photon source based on an InGaAs quantum dot

HRISTINA GEORGIEVA,[1,*] MARCO LÓPEZ,[1] HELMUTH HOFER,[1] NIKLAS KANOLD,[2] ARSENTY KAGANSKIY,[2] SVEN RODT,[2] STEPHAN REITZENSTEIN,[2] AND STEFAN KÜCK[1,3]

[1] *Physikalisch-Technische Bundesanstalt, Bundesallee 100, 38116 Braunschweig, Germany*
[2] *Institut für Festkörperphysik, Technische Universität Berlin, Hardenbergstraße 36, 10623 Berlin, Germany*
[3] *Laboratory for Emerging Nanometrology, Langer Kamp 6, 38106 Braunschweig, Germany*
[*] *hristina.georgieva@ptb.de*

Abstract: We apply an InGaAs quantum dot based single-photon source for the absolute detection efficiency calibration of a silicon single-photon avalanche diode operating in Geiger mode. The single-photon source delivers up to $(2.55 \pm 0.02) \times 10^6$ photons per second inside a multimode fiber at the wavelength of 929.8 nm for above-band pulsed excitation with a repetition rate of 80 MHz. The purity of the single-photon emission, expressed by the value of the 2nd order correlation function $g^{(2)}(\tau = 0)$, is between 0.14 and 0.24 depending on the excitation power applied to the quantum dot. The single-photon flux is sufficient to be measured with an analog low-noise reference detector, which is traceable to the national standard for optical radiant flux. The measured detection efficiency using the single-photon source remains constant within the measurement uncertainty for different photon fluxes. The corresponding weighted mean thus amounts to 0.3263 with a standard uncertainty of 0.0022.

1. Introduction

Single-photon sources (SPS) have the potential to become a new type of standard source for optical radiation [1], as there are so far - in the classical regime - the blackbody radiator and the synchrotron radiation source. The output power P of an ideal SPS, emitting exactly one photon per excitation pulse, is in fact simply given by the formula $P = fhc/\lambda$, where f is the repetition rate of the excitation laser, h is the Planck constant, c is the speed of light, and λ is the wavelength of the emitted radiation. Although it is still difficult to realize an SPS with ideal photon-extraction and collection efficiency, the advantage of high single-photon purity can be directly exploited for the calibration of single-photon avalanche detectors (SPAD), whose detection efficiency (DE) is strongly influenced by the photon statistics. In this way, the otherwise necessary correction of DE when using laser light would be eliminated, which can lead to a reduced calibration uncertainty and a simplified model of the detector response.

A narrow spectral emission bandwidth is an essential prerequisite for the successful calibration of optical radiation detectors, whose DE depends on the wavelength. One possible approach is to implement an SPS with broad spectral emission and then select a specific wavelength through spectral filters. For example, a nitrogen-vacancy center in diamond was fully characterized in a metrological sense [2]. Its emission covers the visible spectral range roughly from 650 nm to 750 nm (half maximum values taken) with a maximum photon flux of 2.6×10^5 photons/s and a single-photon emission purity between 0.1 and 0.23. A relative SPAD calibration through filtering of the emission of a nitrogen-vacancy center with a 19 nm wide bandpass filter has been

#430680 https://doi.org/10.1364/OE.430680
Journal © 2021 Received 6 May 2021; revised 14 Jun 2021; accepted 16 Jun 2021; published 9 Jul 2021

Optics EXPRESS

demonstrated in Ref. [3]. Another approach consists in using an SPS with a narrow linewidth emission, where different types of emitters cover different emission wavelengths. A promising candidate for this purpose is a dibenzoterrylene molecule in an anthracene nanocrystal (DBT:Ac), which emits narrowband photons with strong anti-bunching in the photon statistics, when cooled to cryogenic temperatures [4–7]. A molecule based SPS has been recently applied in quantum radiometry [4]. This SPS delivered up to 1.4×10^6 photons/s at the fiber-coupled detector, while maintaining high purity of the single-photon emission ($g^{(2)}(0) = 0.08 \pm 0.01$) at maximum photon flux. However, due to the continuous wave operation of the source, saturation effects caused by the SPAD dead time were observed, resulting in a count rate dependent DE.

Semiconductor materials are very well suited for the realization of a standard photon source featuring triggered operation, robustness, durability and photostability. Moreover, the emission wavelength of mature InGaAs quantum dots (QDs) in the near infrared enables the calibration of both Si- and InGaAs/InP-SPADs. Highly sophisticated fabrication processes allow the design of structures surrounding the emitting QD, so that high extraction efficiencies and thus high photon fluxes can be obtained [8,9]. In [10], an SPS based on an InGaAs QD has been used for the relative calibration of two Si-SPAD detectors. The source provided photon fluxes up to 3.7×10^5 photons/s at the position of the SPAD under pulsed excitation with a repetition rate of 80 MHz. In this work, we have significantly improved the efficiency of our setup and demonstrate an absolute calibration of a Si-SPAD with an InGaAs QD as a light source. This calibration is a proof of principle for the use of pulsed single-photon emission for a direct comparison of a SPAD with a commercially available low-noise analog detector, which is traceable to the primary standard for optical power, the cryogenic radiometer. With this, we have closed the traceability gap between classical and quantum radiometry.

2. Single-photon source

The setup for the generation of single-photon emission is similar to the one used in [10]. It consists of a home-made confocal microscope with implemented spectral filtering (see Fig. 1). For non-resonant excitation of the QD, a diode laser (PicoQuant, LDH-D-C-850) is used, which is operated in pulsed mode with a repetition rate of 80 MHz and a pulse width of 0.5 ns (full width). Its relatively broadband emission is spectrally filtered with a bandpass filter at 850 nm with a 10 nm wide transmission window. The laser beam is reflected from a dichroic beam splitter (Semrock, 875 nm edge Bright-line) and focused on the sample, which is placed in a cryostat keeping a constant temperature of about 10 K. The QD fluorescence is collected using a high transmission objective (Olympus, LCPLN50XIR, NA=0.65), which has an aberration correction for the 0.2 mm thick cryostat window. The fluorescence light passes through two longpass and two bandpass filters and is then coupled by a high transmission objective (Olympus, LMPLN10XIR) into a multimode optical fiber (62.5 µm core diameter) that serves as a pinhole for confocal imaging. The fiber can be connected to either a spectrometer, a SPAD detector or a fiber based Hanbury Brown and Twiss (HBT) interferometer to analyze spectral properties, to measure photon flux, and to determine the single-photon purity, respectively. Compared to the setup described in [10], we have doubled the overall setup transmission (approx. 49%) by the use of high transmission objectives. The applied aberration correction and improved vibration damping further enhance the overall setup efficiency.

The sample structure, shown in Fig. 2(a), is grown by metal-organic chemical vapor deposition. First, 300 nm GaAs are deposited on a (001) GaAs substrate. Next, 23 pairs of AlGaAs and GaAs layers, with thicknesses of 78 nm and 67 nm, respectively, are forming a distributed Bragg reflector, which reflects the light emitted into the lower hemisphere. A 67 nm thick spacer is grown on top, followed by a thin layer of self-assembled InGaAs QDs and a capping layer with a thickness of 420 nm. Suitable QDs at cryogenic temperatures are selected by cathodoluminescence spectroscopy, whereas electron-beam lithography (EBL) is used to form

Optics EXPRESS

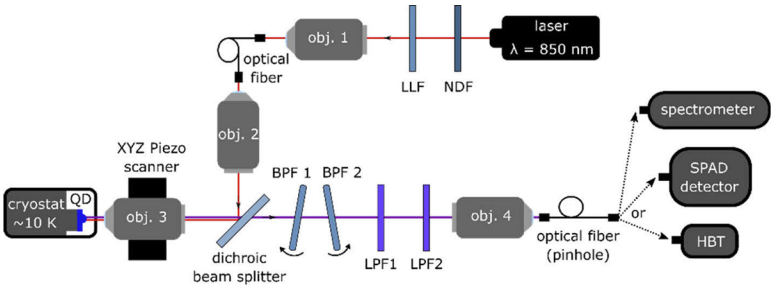

Fig. 1. Self-made confocal setup for the optical characterization of an InGaAs QD emitting at around 930 nm. The sample is in a cryostat. We perform an above-band optical excitation at 850 nm. The excitation power is adjusted with a variable neutral density filter (NDF), whereas the bandwidth of the excitation spectrum is determined by a laser line filter (LLF). The fluorescent emission from the QD is collected by objective 3. It is then spectrally filtered with the help of two bandpass filters (BPF). The laser beam is blocked by two longpass filters (LPF) with a cut-off wavelength of 900 nm. An optical fiber, which serves as a pinhole, can be connected to different devices to measure the spectrum, the photon flux or the single-photon purity.

micromesas at the pre-selected positions. These mesas have a cylindrical shape with a radius between 600 nm and 640 nm and a height of 800 nm. For further information on the used in-situ EBL nanotechnology process we refer to Ref. [11].

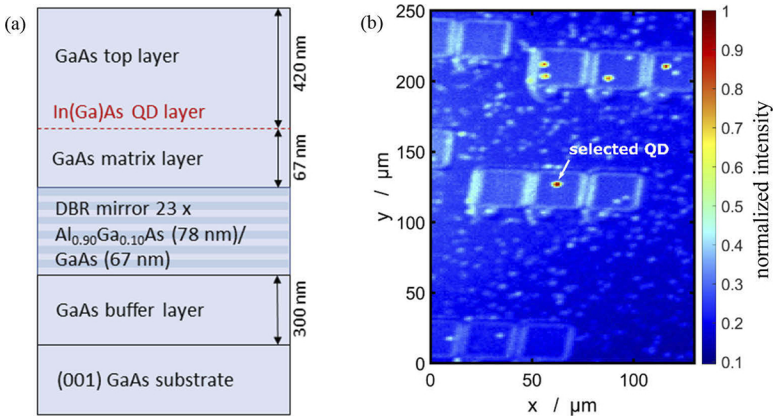

Fig. 2. (a) Schematic of the sample structure. (b) Micro-photoluminescence scan of the sample emission for emission wavelengths above 900 nm. The µPL intensity is significantly higher for QDs integrated into micromesas by in-situ EBL, which nicely illustrates the enhancement of photon extraction by these nanophotonic structures.

A micro-photoluminescence (µPL) scan of the sample with a color-coded emission intensity is shown in Fig. 2(b). Only emission above 900 nm is detected due to the longpass filtering of the fluorescent light that reaches the SPAD detector (Perkin Elmer, SPCM-AQRH-13-FC). The QD layer has been etched away in the rectangular areas, leaving only single QDs inside the micromesas. One of them (indicated in Fig. 2(b)) was selected for further measurements, because it fulfills simultaneously the criteria of having high brightness and good single-photon purity.

The spectrum of the selected QD can be seen in Fig. 3(a). We use the same principle for filtering out one single emission line as in [10], i.e. implementing two identical narrow bandpass filters (Alluxa, 935.0–0.45 OD5), based on thin film interference, with a 0.5 nm wide transmission

Optics EXPRESS

window and a transmission of about 90% each. The resulting filtered spectrum of the SPS is presented in Fig. 3(b), showing one single line at $\lambda = (929.8 \pm 0.1)$ nm with a small shoulder on the long wavelength side, which may be attributed to a second excitonic component of the QD's emission due to a fine-structure splitting of about 70 pm. The spectral linewidth of the photon emission, defined as the full width at half maximum, was determined to 31.4 pm. This value is limited by the resolution of our spectrophotometer (approximately 36 pm for the full width at half maximum). Noteworthy, an emission linewidth below 0.1 nm already enables very accurate radiant flux measurements at a well-defined wavelength.

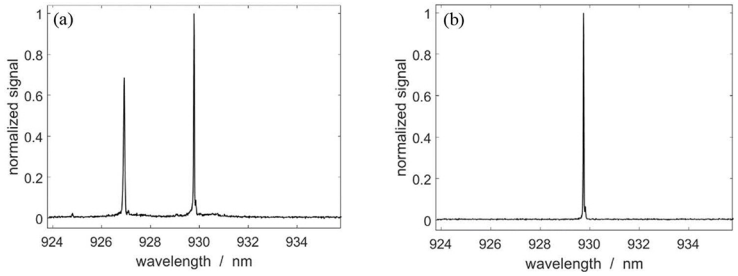

Fig. 3. (a) µPL spectrum of the selected QD. (b) Spectrally filtered QD µPL emission with a wavelength of $\lambda = (929.8 \pm 0.1)$ nm.

Figure 4(a) shows the photon flux at the position of the detector and the single-photon purity in dependence of the applied excitation power. The linear dependence at low excitation implies that the corresponding spectral line belongs to the recombination of an exciton. Here, the photon flux was calculated by dividing the count rate, corrected for dark counts and afterpulsing, by the DE, calibrated in section 3. Due to the improvements in the setup transmission mentioned earlier, we were able to achieve a photon flux of up to $(2.55 \pm 0.02) \times 10^6$ photons per second at an excitation power of 3.5 µW. This photon flux corresponds to a radiant flux of (545 ± 4) fW, which is high enough to be measured with a low-noise analog reference detector, thus allowing an absolute calibration of a SPAD detector by a direct comparison with an analog detector. The overall efficiency η_{total} of our source, including the optical setup for spectral and spatial filtering, can be easily calculated by dividing the photon flux by the repetition rate, thus $\eta_{\text{total}} = 0.0319$. An exemplary measurement of the second-order correlation function $g^{(2)}$ is presented in Fig. 4(b). The obtained $g^{(2)}(\tau = 0)$ value is 0.14 for low excitation powers and reaches 0.24 at saturation.

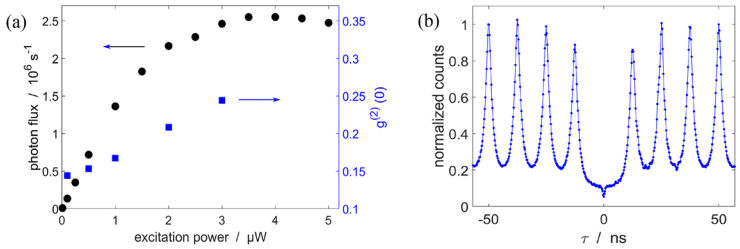

Fig. 4. (a) Photon flux (black circles) and single-photon purity (blue squares) of the InGaAs QD based single-photon source at the position of the SPAD detector. (b) Exemplary second-order correlation measurement for an excitation power of 0.5 µW, which yields $g^{(2)}(0) = 0.15$.

Optics EXPRESS

3. Absolute calibration of Si-SPAD

The calibration of the DE of the SPAD detector was carried out as follows. The output radiant flux P of the SPS was determined with a low-noise fiber-coupled reference detector (Femto, FWPR-20-S) according to: $P = U/s$, where s is the spectral responsivity in volt per watt and U is the voltage. Traceability to the primary standard for optical power, the cryogenic radiometer, is achieved by a calibration of the spectral responsivity. This calibration was conducted according to the double attenuator technique, presented in detail in Ref. [12]. For this purpose, the optical power from a laser (PicoQuant, LDH-D-C-930) at zero attenuation was measured with a calibrated optical power meter (HP, 81530A). Two calibrated variable attenuators were used to vary the optical power in the range between 57 fW and 12.3 pW, and the corresponding voltage was read out from the low-noise analog detector. We did not observe any nonlinearity of the spectral responsivity within the measurement uncertainty in the optical power range stated above. Therefore, the final value for the responsivity $s = (0.5886 \pm 0.0031) \cdot 10^{12}$ VW^{-1} was calculated by taking the weighted mean. The uncertainty of the spectral responsivity considers both the standard deviation of the weighted mean and the repeatability of the calibration results.

The SPAD calibration is performed according to the substitution method. First, the x, y and z coordinates of the selected QD are confirmed with a µPL scan (objective realignment is performed if necessary). The multimode fiber with the spatially and spectrally filtered single-photon emission is connected to the Si-SPAD (Perkin Elmer, SPCM-AQRH-13-FC) to measure the count rate N_{total}, then it is connected to the already calibrated low-noise detector to determine the absolute radiant flux. Since the dark current of the low-noise detector is sensitive to changes in the ambient conditions and may vary over time, its value was measured immediately after the previous step. The last step consists in measuring the count rate a second time with the SPAD for an uncertainty estimation of the temporal stability f_{temp} of our SPS. These steps are repeated for each data point in Fig. 5(a) at different laser excitation powers. The apparent DE η_{SPAD} is determined by:

$$\eta_{\text{SPAD}} = \frac{hc}{\lambda}\frac{s}{U}(N_{\text{total}} - N_{\text{dark}})(1 - p_{\text{a}})\, f_{\text{temp}}\, f_{\text{conn}}. \tag{1}$$

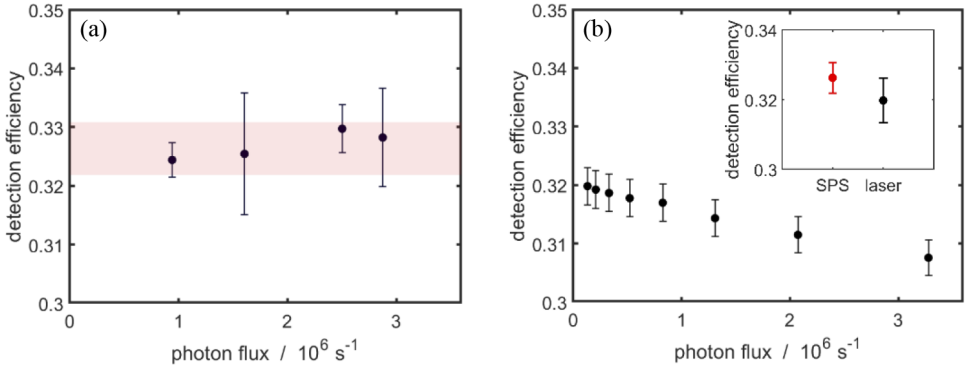

Fig. 5. Si-SPAD detector calibration. (a) Calibration using the spectrally filtered QD emission [for µPL spectrum, see Fig. 3(b)] for a direct comparison with an analog reference detector. The pink area represents the expanded uncertainty ($k = 2$) of the weighted mean. (b) Calibration using a strongly attenuated laser source, where the incoming photon flux has been indirectly determined from a calibration of two variable attenuators. The error bars in (a) and (b) indicate the standard measurement uncertainty. Inset: comparison of the weighted mean of the DE from (a) with the DE from (b) for the lowest measured photon flux, where the error bars show the corresponding expanded uncertainties ($k = 2$).

Optics EXPRESS

Here, h is the Planck constant, and c is the speed of light, both having no uncertainty with the current definition of the SI units. The wavelength of the emitted radiation is denoted by λ, whereas N_{dark} is the dark count rate of the SPAD, and p_{a} is the afterpulsing probability. It was obtained from additional correlation measurements. The value for p_{a} did not change with the photon flux within the measurement uncertainty, which justifies the absence of higher order terms in p_{a} in Eq. (1). Finally, the term f_{conn} takes into account the change of the coupling losses of the FC/PC connector, estimated to 0.5%. This is an empirical value confirmed by connecting and disconnecting the fiber patch cord several times and looking at the relative change of the count rate from a SPAD with a stable laser as a light source.

It is important to note that we are using the conventional definition of the apparent DE, given by the measured count rate, corrected for dark counts and afterpulsing, divided by the incident photon flux. This value depends on the properties of the light source and of the SPAD detector and is in general count rate dependent.

An exemplary measurement uncertainty budget of the third data point in Fig. 5(a) is shown in Table 1. The largest contribution stems from the temporal stability of the QD emission. The traceable calibration of the spectral responsivity of the low-noise analog detector as well as the change of the coupling loss of the FC/PC connector are two further significant sources of uncertainty. The smallest uncertainty contribution arises from the dark count rate, since the high count rate leads to an excellent signal-to-noise ratio. The uncertainty in the wavelength has also a small contribution to the overall uncertainty of the DE because of the very narrow linewidth of the QD emission.

Table 1. Measurement Uncertainty Budget for the Calibration of a Si-SPAD Detector Against a Low-Noise Analog Reference Detector for the Third Data Point in Fig. 5(a)

Source of Uncertainty	Value	Relative Standard Uncertainty (%)	Distribution	Contribution (%)
Planck constant h	$6.62607015 \times 10^{-34}$ J s	0	-	0
Speed of light c	299792458 m s^{-1}	0	-	0
Wavelength λ	929.8 nm	0.01	Rectangular	0.01
Spectral responsivity s	0.5886×10^{12} V W^{-1}	0.53	Standard	17.97
Voltage U	0.3082 V	0.13	Standard	1.03
Count rate N_{total}	825500 s^{-1}	0.08	Standard	0.39
Dark count rate N_{dark}	231 s^{-1}	1.02	Standard	0.002
Afterpulsing probability p_{a}	0.0208	4.81	Standard	0.68
Temporal stability f_{temp}	1	0.99	Rectangular	63.73
Connect/disconnect fiber factor f_{conn}	1	0.50	Rectangular	16.19
Combined uncertainty u_{c}		1.24	Standard	100

The results of the DE calibration are shown in Fig. 5(a), where the DE is plotted against the photon flux impinging on the detection area for the calibration using the QD based SPS. The different size of the error bars is mainly due to variations of the uncertainty of the temporal stability f_{temp}, which was estimated independently for each data point. Note that the calibration was performed on a different day than the recording of the saturation curve, which explains the nonidentical maximum photon flux. As can be seen, the measured DE is independent of the incoming photon flux within the stated uncertainties. We determined a weighted mean of 0.3263 ± 0.0022 for the apparent DE. One would expect a small decrease with increasing photon flux because of the dead time of the SPAD detector. In order to quantify this contribution, we derived an equation (based on the model in Ref. [13]) describing the dead time effect for an ideal

Optics EXPRESS

SPS with an efficiency of φ/f:

$$\eta_{\mathrm{SPAD}} = \frac{\eta_0}{1 + \mathrm{Int}(fD)\frac{\varphi}{f}\eta_0}, \tag{2}$$

where η_0 is the intrinsic detection efficiency, φ is the photon flux, and Int is the integer part of the product of source frequency f and SPAD dead time $D = (29.2 \pm 0.2)$ ns. Therefore, we expect an absolute change of the apparent DE by 0.005 between the first and last data point in Fig. 5(a). However, such a small change lies within the expanded measurement uncertainty of each of the four DE values. The imperfection of our SPS, namely the nonzero second-order correlation at zero delay, could also influence the apparent DE. The magnitude of this change depends on the product $\varphi \cdot g^{(2)}(0)$. With the use of the equation from Ref. [10] and with the data from Fig. 4(a) we estimate a maximum decrease of the apparent DE with the photon flux by about 0.4%, which is clearly below the relative standard uncertainties (between 0.91% and 3.18%) in Fig. 5(a).

In Fig. 5(b), the measured DE is shown for a calibration using attenuated laser pulses (PicoQuant, LDH-D-C-930) with the same repetition rate of 80 MHz. A decrease of the measured DE with increasing photon flux can be observed, as expected from the photon statistics of the laser light in combination with the dead time of the Si-SPAD detector. The saturation of the count rate at high optical powers is enhanced by the presence of multiphoton events due to the Poisson nature of the laser emission.

Both calibration methods in Fig. 5 yield consistent results at low photon fluxes, where dead time and photon statistics have a negligible effect. In the inset in Fig. 5(b), the weighted mean from the calibration with the SPS is compared with the DE at the lowest photon flux measured with an attenuated laser. The values agree within their expanded uncertainties ($k = 2$). Both QD and laser have about the same emission wavelength: 929.8 nm and 930 nm, respectively. The QD possesses a smaller spectral linewidth; its pulse width in the time domain is determined by the decay time of the excited state (1.7 ns), which could be improved by exploiting the Purcell effect in a cavity-enhanced SPS [8,14,15]. Just by improving the temporal stability of the QD emission it would be possible to reduce the overall measurement uncertainty by a factor of two, so that it becomes comparable or even lower than the uncertainty of the calibration with attenuated laser light.

The presented calibration method has several advantages over the classical method with attenuated laser light. The QD emission falls directly in the desired photon flux range, whereas laser light has to be attenuated by about ten orders of magnitude for traditional calibration methods [12,16], which implies an additional calibration of the attenuators contributing to the measurement uncertainty. Moreover, pulsed QD operation with a repetition period below the dead time of the SPAD detector would completely remove any saturation effects caused by its dead time. Therefore, this calibration method has the potential of reaching a simple linear dependence between incoming photon flux and measured count rate which would further reduce the measurement uncertainty. In contrast, even for $fD < 1$, the Poisson statistics of laser light lead to a strong saturation of the count rate at high photon fluxes because of the large mean photon number. This saturation effect is hard to be precisely modelled and limits the usable detection range.

4. Summary

We have developed a pulsed InGaAs QD based single-photon source applied for the direct calibration of a single-photon avalanche detector against a classical analog reference detector. The single-photon source was metrologically characterized with respect to its total radiant flux, which was up to $(2.55 \pm 0.02) \times 10^6$ photons/s, corresponding to (545 ± 4) fW at an emission wavelength of $\lambda = 929.8$ nm, and with a single-photon purity of $g^{(2)}(0) < 0.25$. This development can be considered as a significant improvement in the field of quantum radiometry, since, due

Optics EXPRESS

to the pulsed operation and sub-Poisson statistics of the light source, any count rate saturation effects of the single-photon detector are diminished.

Funding. Deutsche Forschungsgemeinschaft (390837967, Re2974/23-1, RTG 1952); European Metrology Programme for Innovation and Research (17FUN06 SIQUST).

Acknowledgments. This work was funded by the project EMPIR-17FUN06 SIQUST. This project received funding from the EMPIR program co-financed by the Participating States and from the European Union Horizon 2020 research and innovation program. We gratefully acknowledge the support of the Braunschweig International Graduate School of Metrology B-IGSM and the DFG Research Training Group 1952 Metrology for Complex Nanosystems. This work was also supported by the Deutsche Forschungsgemeinschaft (DFG, German Research Foundation) under Germany's Excellence Strategy—EXC- 2123 QuantumFrontiers—390837967 and via the project Re2974/23-1.

Disclosures. The authors declare no conflicts of interest.

Data availability. Data underlying the results presented in this paper are not publicly available at this time but may be obtained from the authors upon reasonable request.

References

1. J. Y. Cheung, C. J. Chunnilall, E. R. Woolliams, N. P. Fox, J. R. Mountford, J. Wang, and P. J. Thomas, "The quantum candela: a re-definition of the standard units for optical radiation," J. Mod. Opt. **54**, 373–396 (2007).
2. B. Rodiek, M. López, H. Hofer, G. Porrovecchio, M. Šmid, X.-L. Chu, S. Götzinger, V. Sandoghdar, S. Lindner, C. Becher, and S. Kück, "Experimental realization of an absolute single-photon source based on a single nitrogen vacancy center in a nanodiamond," Optica **4**, 71–76 (2017).
3. W. Schmunk, M. Rodenberger, S. Peters, H. Hofer, and S. Kück, "Radiometric calibration of single photon detectors by a single photon source based on NV-centers in diamond," J. Mod. Opt. **58**, 1252–1259 (2011).
4. P. Lombardi, M. Trapuzzano, M. Colautti, G. Margheri, I. P. Degiovanni, M. López, S. Kück, and C. Toninelli, "A molecule-based single-photon source applied in quantum radiometry," Adv. Quantum Technol. **3**, 1900083 (2020).
5. G. Wrigge, I. Gerhardt, J. Hwang, G. Zumofen, and V. Sandoghdar, "Efficient coupling of photons to a single molecule and the observation of its resonance fluorescence," Nat. Phys. **4**, 60–66 (2008).
6. A. A. L. Nicolet, C. Hofmann, M. A. Kol'chenko, B. Kozankiewicz, and M. Orrit, "Single dibenzoterrylene molecules in an anthracene crystal: spectroscopy and photophysics," Chem. Phys. Chem. **8**, 1215–1220 (2007).
7. B. Kozankiewicz and M. Orrit, "Single-molecule photophysics, from cryogenic to ambient conditions," Chem. Soc. Rev. **43**, 1029–1043 (2014).
8. H. Wang, Y.-M. He, T.-H. Chung, H. Hu, Y. Yu, S. Chen, X. Ding, M.-C. Chen, J. Qin, X. Yang, R.-Z. Liu, Z.-C. Duan, J.-P. Li, S. Gerhardt, K. Winkler, J. Jurkat, L.-J. Wang, N. Gregersen, Y.-H. Huo, Q. Dai, S. Yu, S. Höfling, C.-Y. Lu, and J.-W. Pan, "Towards optimal single-photon sources from polarized microcavities," Nat. Photonics **13**, 770–775 (2019).
9. N. Tomm, A. Javadi, N. O. Antoniadis, D. Najer, M. C. Löbl, A. R. Korsch, R. Schott, S. R. Valentin, A. D. Wieck, A. Ludwig, and R. J. Warburton, "A bright and fast source of coherent single photons," Nat. Nanotechnol. **16**, 399–403 (2021).
10. H. Georgieva, M. López, H. Hofer, J. Christinck, B. Rodiek, P. Schnauber, A. Kaganskiy, T. Heindel, S. Rodt, S. Reitzenstein, and S. Kück, "Radiometric characterization of a triggered narrow-bandwidth single-photon source and its use for the calibration of silicon single-photon avalanche detectors," Metrologia **57**, 055001 (2020).
11. S. Rodt and S. Reitzenstein, "High-performance deterministic in situ electron-beam lithography enabled by cathodoluminescence spectroscopy," Nano Ex. **2**, 014007 (2021).
12. M. López, H. Hofer, and S. Kück, "Detection efficiency calibration of single-photon silicon avalanche photodiodes traceable using double attenuator technique," J. Mod. Opt. **62**, 1732–1738 (2015).
13. H. Georgieva, A. Meda, S. M. F. Raupach, H. Hofer, M. Gramegna, I. P. Degiovanni, M. Genovese, M. López, and S. Kück, "Detection of ultra-weak laser pulses by free-running single-photon detectors: modeling dead time and dark counts effects," Appl. Phys. Lett. **118**, 174002 (2021).
14. S. Kolatschek, S. Hepp, M. Sartison, M. Jetter, P. Michler, and S. L. Portalupi, "Deterministic fabrication of circular Bragg gratings coupled to single quantum emitters via the combination of in-situ optical lithography and electron-beam lithography," J. Appl. Phys. **125**, 045701 (2019).
15. X. Ding, Y. He, Z.-C. Duan, N. Gregersen, M.-C. Chen, S. Unsleber, S. Maier, C. Schneider, M. Kamp, S. Höfling, C.-Y. Lu, and J.-W. Pan, "On-demand single photons with high extraction efficiency and near-unity indistinguishability from a resonantly driven quantum dot in a micropillar," Phys. Rev. Lett. **116**, 020401 (2016).
16. T. Gerrits, A. Migdall, J. C. Bienfang, J. Lehman, S. W. Nam, J. Splett, I. Vayshenker, and J. Wang, "Calibration of free-space and fiber-coupled single-photon detectors," Metrologia **57**, 015002 (2020).